LES-CHT for Smooth and Micro-structured Walls

L. He
Department of Engineering Science,
University of Oxford,
Oxford, OX2 0ES, United Kingdom

Abstract

Aerothermal flow design/optimization is normally carried out by changing the shape of solid wall bounding the flow. It has been well recognised that flow characteristics and performance can also be strongly influenced by surface finish (random roughness or regular micro-structures). The emergence of additive manufacturing (AM) technologies has raised the prospect of 'Surface Design', where both surface-shape and local surface-finish may be designed for performance gains. The question then becomes: what shape & patten of additively manufacturable surface microstructures (presently and/or in future) shall we want? This question may only be answerable if we have the local resolving capability for a micro-structured surface subject to a nonuniform bulk flow. The primary computational challenges arise from the two disparate micro (surface finish element) and macro (bulk flow) length scales. For fluid-solid coupled conjugate heat transfer (CHT) analysis, the acute time-scale disparity between the two domains also needs to be dealt with, particularly for turbulence-resolving LES where a very small time-step has to be used.

We address the scale disparity issues by multi-scale methods. On the one hand for long transients as in practical start-up/shutdown and flexible operation processes, a 'dual time-marching' procedure is introduced to enable an efficient and accurate transient CHT solution. On the other hand, for scale-resolving turbulent flow disturbances in high frequencies, the hugely mismatched timescales in fluid and solid are effectively realigned by treating the solid domain in frequency domain. As such, the time-averaged (the zeroth harmonic in time) is effectively obtained in the same way as a steady CHT problem. A distinctive semi-analytical harmonic transfer function makes it possible for unsteady wall temperatures to be directly obtained from the near-wall fluid temperature harmonics. Quite remarkably, we can then get unsteady wall temperatures without even solving an unsteady temperature field in solid domain. Consequentially, the solid domain is effectively solved as a steady conduction problem in its own time step, several orders of magnitude larger than the physical time step used in the fluid domain. The two-scale framework introduced earlier is also applied to solving near wall flows around micro-structure blocks. Furthermore, the two-scale method is extended to the solid domain for solving the steady conduction equation. High gradient 'hot spot' temperatures around micro-structures in solid near-wall region are now well resolved efficiently in the LES-CHT analysis.

The results of two-scale solid conduction solutions also serve to demonstrate unambiguously the working of the 'mesh-informed' source-terms. A solid-only setting having nothing to do with Reynolds stresses underlines the key role played by numerical discretization errors when a near-wall coarse-mesh is adopted (for cost-benefit) as in common wall modelled (or wall-function conditioned) LES. Because of the inherent numerical discretization errors in coarse-mesh nearwall flow solutions, it is argued that a correct Reynolds stress field (regardless of how it is obtained) may not produce a correct flow field. Nor is a correct wall-function (regardless of how it originates) expected to condition a coarse-mesh solution consistently leading to a correct flow field.

Background and Main Issues of Interest

1.1. Conjugate Heat Transfer

For gas turbines/aero-engines, designers need to deal with aerodynamic performance, as well as thermal mechanical integrity and lifespan of hot-end components. Typically, aerothermal design and analysis development depend on the capability of scaling relevant parameters from different flow speeds and/or temperature conditions. At the heart of the convective heat transfer and scaling methods is Newton's Law of Cooling:

$$q = h(T_f - T_w) \quad (1)$$

where q is a surface heat flux, T_f and T_w are the temperatures of fluid and solid wall, respectively.

In general, the central point in convective heart transfer tends to be the heat transfer coefficient (HTC) h. A basic assumption of an HTC based method is that convective heat transfer is predominantly determined by fluid mechanics/aerodynamics, and heat transfer at a wall boundary has negligible feedback to the wall bounded flow

For practical applications of thermal fatigue life designs and durability analysis for heating/cooling sensitive components, temperature distributions in the solid are needed. An HTC distribution over a solid surface can be obtained first based on either an empirical correlation (typically based on Nusselt number for scaling to different geometrical and working conditions), an experimental measurement, or a numerical simulation in the fluid-domain-only setting. It can then be used to solve a conduction equation in a solid-domain-only setting at convective boundary conditions with the HTC and fluid temperature commonly taken as invariant to the solid wall temperature. This decoupled HTC approach is in line with the basic assumption that the wall heat transfer does not affect fluid dynamics which dictates convective heat transfer.

There are two main issues of interest in relation to the cooling law (Eq.1). Firstly, the conventional HTC is only accurately applicable for isothermal wall (T_w=constant for entire wall surface), e.g. see Moffat 1998 [1]. A theoretical analysis on this issue and some related computational case studies for non-isothermal walls are presented by He 2023 [2].

Secondly, the 'feedback' effects of wall heat transfer on near-wall flow field may be non-negligible at some conditions of practical interest. Here is an example of how wall heating on a rotating cavity may destabilise otherwise well-balanced local near-wall flow patterns, leading to thermally-driven turbulence generation, as shown in Fig.1 (Hickling & He 2023 [3]).

In this case, the original experimental thermal setup with both a radial heating on the cavity shroud and an axial heating on the cavity disk is decomposed into two test cases with either a radial heating or an axial heating respectively. The two 'isolated' cases help highlight how local wall heat transfer can significantly affect corresponding flow instabilities and turbulence generation. For the axial heating setup (Figs.1a, 1c). the reference case (without the heating) sees a self-organised counter-rotating pairing vortices pattern supported by the balance between a circumferential pressure gradient of the vortices and the Coriolis force due to radial flows between the vortices and the cavity rotation. Once the disc heating is introduced however, the density drop due to heating reduces the Coriolis force, resulting in a destabilising effect on a radial outflow part, leading to large-scale turbulent structures emerging locally (Fig.1c). For a radial inflow region, there is an opposite

(stablishing) mechanism. Consequently, we see a distinctive high-low turbulence radial strips in the bulk flow moving slowly (at a 5-10% rotor speed) relatively to the rotor.

For the radial heating setup (Figs.1b, 1d), a baseline unheated case has a radial momentum balance in the region near outer casing (shroud): the radial pressure gradient should provide sufficient centrifugal force to sustain tangential fluid movement. For a cyclonic vortex with a lower pressure at its centre, the local radial pressure on the shroud should thus be relatively high. With the radial heating added, the lower circumferential momentum near the heated casing can lead to a momentum imbalance in form of excess local radial pressure force. This promotes roll-up vortical structures near the shroud, leading to those 'thermal streaks' visible on the shroud wall (highlighted in circle, Fig.1b).

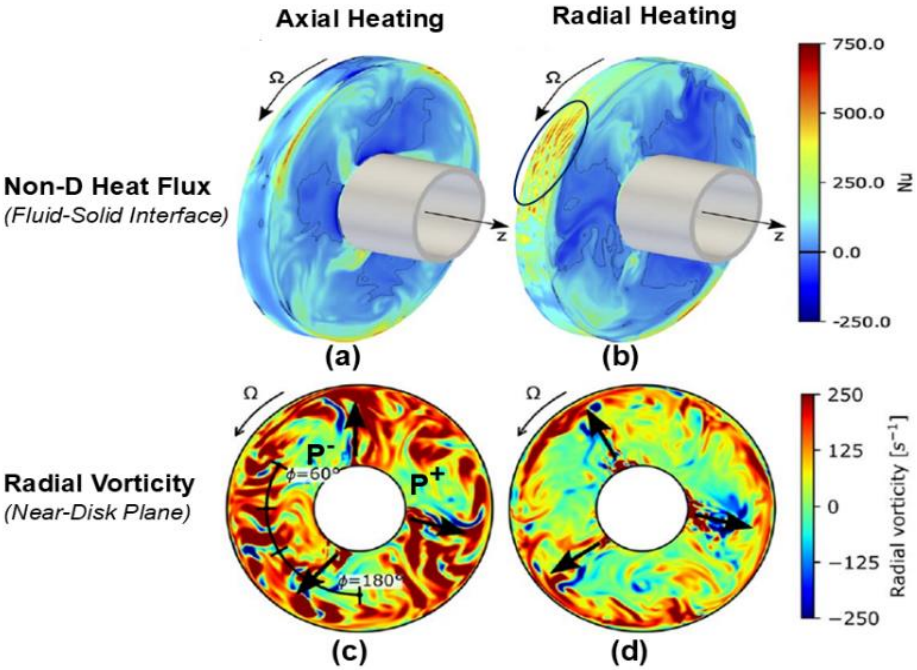

Figure 1: Thermally driven Turbulent Flows in Rotating Cavity [3].

Given the strong dependence of these thermally-driven turbulent flows on the wall temperature, the results underline the need for coupled CHT solutions in conjunction with turbulence-resolving LES.

In the past few decades, development of computational fluids dynamics (CFD) has greatly enhanced capabilities in predicting detailed flow field features and detailed HTC distributions for complex practical configurations. Fluid-solid coupled Conjugate Heat Transfer (CHT) methodologies and working methods have also been extensively developed. However, CHT methods also face challenges, particularly when applied to transient CHT problems chiefly due to the time-scale disparity between fluid and solid, as discussed in He and Oldfield 2011 [4], He 2023 [5]). These issues should be addressed in developing advanced CHT methods particularly in conjunction with high-fidelity scale-resolving LES solvers.

1.2. Wall Roughness: Challenges and Opportunities

Fluid flow and convective heat transfer for micro-structured surfaces are important in many practical applications. Impact of general stochastic roughness on friction drag and heat transfer performance is a subject of long-standing interest. There have been many efforts in correlating increased friction and heat transfer to the equivalent roughness parameters (e.g. Jimenez 2004 [6]). The current

consensus is that flow velocity in an outer-wall region can be reasonably well correlated to a general similarity profile for smooth and roughened surfaces, as first postulated by Townsend (1976) [7]. The near-wall flow as well as the main scaling parameters are however dependent on more detailed roughness geometry (Flack and Shultz 2004 [8]). Comprehensive understanding of how roughness affects boundary layer aerothermal performance is still lacking, particularly for relatively large roughness scales. Direct numerical simulations (e.g. Thakkar et al 2018 [9]) help understand roughness characteristics. It is shown that resolving detailed roughness micro-structure geometries may be needed in many cases for better characterization of roughness behaviour and performance prediction than the conventional largely empirical treatment, as pointed out by Flack 2018 [10].

The motivation in resolving surface micro-structures is also heightened by the development of additive manufacturing (AM). AM-made components tend to exhibit surface finishes deviating significantly from conventional roughness (e.g. Snyder and Thole 2020 [11]). The associated influences on performance need new predictive tools. It has also been indicated that shape and patterns of regular surface micro-structures considerably affect the aerothermal performance (e.g. Kapsis and He, 2019 [12], Kapsis et al 2020 [13], Wilkin et al 2022 [14]). The continuous AM development raises significant potential for future exploitation of surface finish ('manufacturable roughness') by design and advanced manufacturing. The prospect of 'Surface Design' also motivates the present work in following a pathway to develop accurate and efficient methods to resolve, rather than to model, surface micro-structures. A closely related topic area is in cooling technologies: e.g. film-cooling [15-17], effusion cooling [18-20]), and transpiration cooling [21],[22]. The major common challenge in all these problems arises from the large scale disparity between corresponding micro-structures and bulk flows.

Surface roughness is known to affect laminar-turbulent transition. It is of interest to see the influence of the wall temperature condition. Such influence is examined for a low-speed flow over wall surface with an array of micro-structures (Campanaro and He 2023 [23]). Fig.2 shows the LES results for two Reynolds numbers (Re_r is based on the bulk flow condition and radius of hemispheric micro-element) at an adiabatic wall condition. The transition happens at around Re_r=5000.

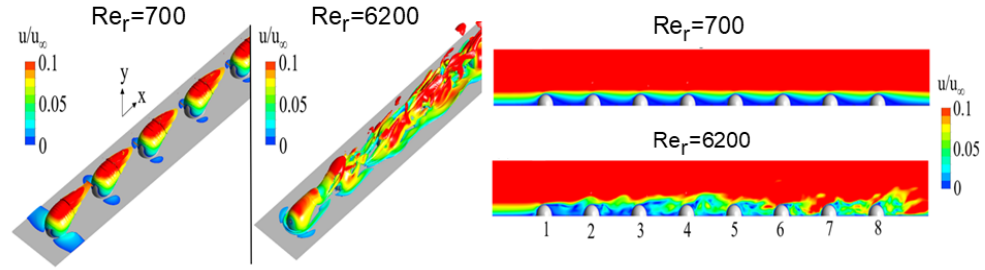

(a) Flow Patterns (laminar *vs.* Turbulent) at Two Reynolds Numbers

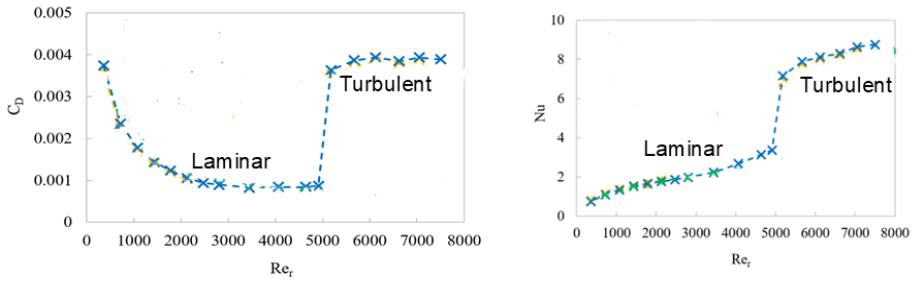

(b) Drag (C_D) and Heat Transfer (Nu) Variation with Reynolds Number

Figure 2: Flow Pattern and Performance-Re_r Characteristics (*Adiabatic Wall*) [23].

We then look at what happens when wall heat transfer is added. The case is examined at different wall temperatures (T_w specified to be a constant over wall boundary) to give different temperature ratios T_w/T_{01} for a fixed inlet flow stagnation temperature T_{01}. At a Reynold number Re_r=4000, a near adiabatic case (TR=T_w/T_{01}=0.98) is clearly laminar (Fig.3a) as expected from the adiabatic characteristics (Fig.2b). But at the same Reynolds number, a cooled wall at TR=0.5 becomes seemingly turbulent (Fig.3b). The flow characteristics demonstrate very pronounced impact of the wall heat transfer on both drag (Fig.3c) and in turn on the heat transfer itself (Fig.3d).

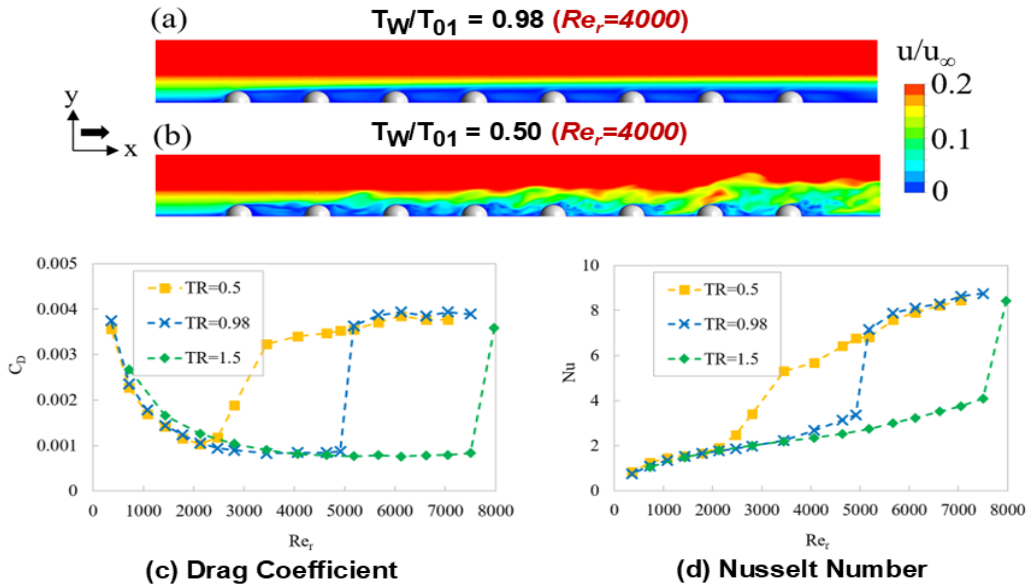

Figure 3: Transition Flow at Re_r = 4000 and Performance-Re_r Characteristics (*Diabatic*) [23].

The strong dependence on the wall temperature underlines the need for a coupled CHT solution. We thus will have to consider both scale disparities in space as well as in time when the fluid-solid thermal coupling is included.

1.3. Lecture Outline

Given the background and key relevant issues as introduced above, the rest of the lecture is organised as follows.

Section 2: We will conduct some simple scaling analysis of the time-scale disparity between solid and fluid, relevant to conjugate heat transfer for both smooth and rough walls in general. In particular, the implication for time-dependent transient CHT is underlined.

Section 3: For the time-scale disparity, two approaches will be presented for unsteady CHT.

i) For large scale long transients, a multi-scale time-integration method is introduced.

ii) For high frequency turbulent flow fluctuations, a time-frequency domain approach is developed for scale-resolving LES based CHT.

Second 4: For the spatial scale disparity between micro-structures and macro bulk flow, the two-scale method is applied to the flow side of the micro-structure surface. Furthermore, the method is extended to solid domain, leading to efficient and accurate source-term driven coarse-mesh conduction solution of small-scale nonuniform temperature field in solid as part of the LES-CHT.

Section 5: we will look at a few case examples, before closing the lecture with some final remarks.

2. Time-scale Disparity: Implications for Unsteady CHT

Consider a fluid domain of a characteristic length L_f and a solid domain of a characteristic length L_s. Subscripts 'f' and 's' are used to denote the parameters for fluid and solid domains respectively. If the fluid part is dominated by convection at a characteristic velocity V_f, the fluid time scale ('throughflow time') is estimated as,

$$\tau_f = \frac{L_f}{V_f} \tag{2}$$

For solid conduction, the time scale τ_s can be taken simply by scaling the 1-D unsteady conduction equation, leading to $\tau_s = L_s^2 / \alpha_s$ (for solid thermal diffusivity α_s). The solid conduction (diffusion) time scale is thus,

$$\tau_s = \frac{Cp_s \rho_s L_s^2}{k_s} \tag{3}$$

The difference in time scales between two domains can be measured by the ratio,

$$\frac{\tau_s}{\tau_f} = \frac{Cp_s \rho_s L_s^2}{k_s} \frac{V_f}{L_f} \tag{4}$$

which can be rearranged as (He 2023 [5]):

$$\frac{\tau_s}{\tau_f} = \left(\frac{Cp_s}{Cp_f}\right)\left(\frac{\rho_s}{\rho_f}\right)\left(\frac{k_f}{k_s}\right)\left(\frac{L_s}{L_f}\right)^2 (Pr_f)(Re_{L_f}) \tag{5}$$

For an order of magnitude estimate, take a typical stainless steel as the solid, air at the ambient condition as the fluid, and $L_s = 0.1\, L_f$. We then find:

$$\left(\frac{Cp_s}{Cp_f}\right) \sim O(10^0);\ \left(\frac{\rho_s}{\rho_f}\right) \sim O(10^4);\ \left(\frac{k_f}{k_s}\right) \sim O(10^{-3});\ \left(\frac{L_s}{L_f}\right)^2 \sim O(10^{-2});\ Pr_f \sim O(10^0)$$

The scales then lead to

$$\frac{\tau_s}{\tau_f} \sim O(10^{-1}) Re_{L_f} \tag{6}$$

Thus for a typical Reynolds number of practical interest, Re_{L_f} ~ 10^5, we shall have,

$$\tau_s/\tau_f \sim 10^4 \tag{7}$$

This time-scale ratio is similar to the time-step ratio between solid and fluid domains based on the numerical stability and accuracy for the two domains, as estimated by He and Oldfield [4].

The implications of this time scale disparity may be better understood when considering it in conjunction with how a numerical solution method would normally function. A CHT for a fluid-solid coupled domain is an initial and boundary condition problem. For a numerical solution method, its task is to iteratively reduce errors so that a converged solution will satisfy both the discrete equations for all interior mesh points/cells and the boundary conditions on all boundary points (and at fluid-solid interfaces). In the context of a time-marching solution method, all numerical errors will manifest in transient disturbances. The time marching solution can effectively function by driving these numerical transients out of the domains similarly to propagating physical unsteady disturbances, e.g. propagating acoustic/pressure waves upstream (in a subsonic flow) and downstream at corresponding acoustic velocities, and convective vorticity and entropy disturbances downstream at local flow velocities.

Computational costs for a converged solution are measured by the number of mesh points in the domains and by the number of time steps needed to drive those numerical error disturbances out of the fluid and solid domains. The number of time steps $N_{\Delta t}$ required is thus influenced by the domain size and the speed at which the transient disturbances are propagated, as well as by the size of the time step Δt. For a fluid domain, major error disturbances tend to be advected at the flow velocity, thus we have $N_{\Delta t_f} = \frac{(L_f/V_f)}{\Delta t_f} = \frac{\tau_f}{\Delta t_f}$. Similarly, for the solid domain, the equivalent error propagation speed is L_s/τ_s for a given domain size and material properties, we thus have $N_{\Delta t_s} = \frac{\tau_s}{\Delta t_s}$.

For steady CHT, the time scale disparity does not make a substantive difference. As both the time scale and the time step size are in proportion for either the fluid or the solid domain, the numbers of time steps for the two domains for a steady CHT are thus comparable to their counterpart for a separate decoupled fluid-only or solid-only solution respectively.

For an unsteady CHT however, there is an acute problem. There are two conflicting requirements that must be satisfied to solve the unsteady CHT problem.

i) The CHT time step needs to be small enough for resolving the smallest disturbance of the coupled domain, which is the fluid unsteadiness in this case. Thus for time-accuracy, we need,

$$\Delta t_{CHT} = \Delta t_f \tag{8}$$

ii) The total time scale to be covered needs to be large enough to allow enough time for initial transients and unsteady physical disturbances to propagate through the domain. Otherwise, some boundary conditions are not enacted and the CHT solution will not converge. Thus, for the time-consistence and CHT solution convergence, we need,

$$\tau_{CHT} = \tau_s \tag{9}$$

Given the dual requirement of time accuracy and time consistency (Eq.8, Eq.9), the corresponding number of time steps needed for the unsteady time-domain CHT solution should be,

$$N_{CHT} = \frac{\tau_s}{\Delta t_f} = \frac{\tau_s}{\tau_f} N_{\Delta t_f} \tag{10}$$

Hence, N_{CHT} can be amplified by a factor ~10^4 times of that for a fluid-only or solid-only solution. Therefore, a direct time-consistent and time-accurate CHT will be prohibitively time consuming and practically infeasible.

It should be noted that there have been various efforts to explore potential options to circumvent or mitigate the challenge arising from the time-scale disparity. The possibility of moderating the time scale disparity with a modified solid material is explored by Diefenthal et al [24], and Łuczynski et al [25], which can lead to considerable speedup of the transient CHT, but may also be associated with some non-negligible and non-physical fluctuations in the solid (Maffulli et al [26]). A mixed approach (Oh et al [27]) is also employed to first use modified material properties to provide more rapidly an approximate initial field. Next, a further time marching of the solution with the correct solid material properties is carried out at the small but physically consistent fluid time-step towards the final solution. Alternatively, a hybrid approach can be formulated to solve a steady CHT problem to provide the base steady temperature field, and a time-domain CHT for a

fluctuating temperature component in solid domain, is time-integrated at a small fluid time step (Koren et al [28]).

Caution should be taken with respect to these mixed/hybrid approaches in the context of the time-accuracy and time-consistency (solution convergence) requirements as discussed for Eqs.8 & 9. Regardless of how an initial or baseline flow field is obtained, the time-domain solution itself is still an initial value problem subject to errors of the initial field. When the time-domain solution in the solid domain is marched forward in time in a time-accurate manner, the initial erroneous disturbances will be propagated in the same way as physical unsteady disturbances. Thus, both initial error transients and physical unsteadiness will still have to travel through the whole domain before a converged solution is reached. As such, the time-domain part of the CHT solution will still be subject to the dual time-consistence and time-accuracy requirement and a huge number of time steps will still be required (Eq.10). Otherwise, the accuracy and/or convergence of the time-domain CHT solution will be compromised. In general, the dual time accuracy-consistence requirement (Eqs.8 & 9) in terms of the fluid-resolution and solid-convergence is believed to be the primary challenge in advanced CHT development, particularly for high fidelity scale-resolving turbulent flow solution based CHT methods.

In the following section, we will introduce two multiscale methods in order to circumvent this acute challenge arising from time-scale disparity. First, we will present a multi-scale time-integration method developed for applications of long timescale turbomachinery transient operations. Secondly, for short scale high frequency turbulent fluctuations, a Fourier spectral method is introduced to incorporate a scale-resolving turbulence solver in an efficient and accurate LES-CHT solution. The two methods complement each other covering a whole time-scale range.

3. Multi-scale Methods for Unsteady CHT

3.1. Dual Time-marching for Long Transient Process

A common assumption adopted in conventional approaches to transient CHT problems is the 'quasi-steady' treatment of the fluid domain. The huge time scale disparity seems to provide a natural justification for a fluid-solid scale separated strategy as adopted in a common loosely coupled CHT approach (e.g. Sun et al [29], Errera and Baqué [30]). In a loosely coupled approach for a transient CHT process, the unsteadiness is only retained in solid domain. A steady (or time-averaged) fluid side will couple with the solid side at each large time step for resolving the transient solid conduction. Given that the fluid domain may be subject to a wide range of time scales, this quasi-steady treatment for the fluid domain may become questionable when there are large-scale low-frequency flow disturbances. Also relevant is that the fluid-solid system may be subject to fast transients during only a certain part (e.g. a local initial ramp-up phase) in an otherwise slow overall process. The recognition of the restrictions of the existing quasi-steady flow assumption for transient CHT has motivated a multiscale time-integration method (He and Fadl 2017 [31]). Here the primary intent is to eliminate the quasi-steady assumption for the fluid domain solution, so that we include the interactions between short/medium scales and large scales, but do so in an efficient manner.

We start with a conventional scale-dependent flow decomposition,

$$\boldsymbol{U}(x,t) = \widetilde{\boldsymbol{U}}(x,t) + U'(x,t) \tag{11}$$

$\tilde{U}$ is the flow variable after a low-pass filtering so that it only contains long wavelength disturbances comparable with the large time scales of unsteady conduction in the solid domain. U' represents the remaining small-scale fluctuations (Fig. 4). The time-integration for the small-scale fluctuations (Fig.14c) will be challenging due to far too many very small time-steps due to the high resolution required and the very long time period of a slow transient process.

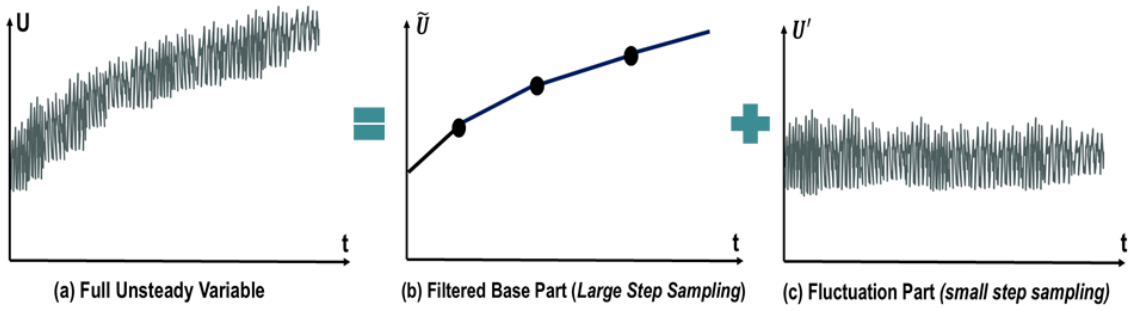

Figure 4: Scale-dependent Temporal Decomposition

To address the challenges faced by the conventional time-scale based decomposition, we adopt a dual time marching approach (He and Fadl [31]. In a discrete time domain, a large-scale time instant t_M is taken corresponding to a temporal resolution required for solid conduction. Because of the time-scale disparity, it is assumed that the time-accurate fluid solution would only need to be carried out around a discrete large-scale time instant, similar to that shown in Fig.4b. However, a small-scale time instant t_n is taken only around a fixed large-scale time instant t_M,

$$t = t_M + t_n \tag{12}$$

Effectively, the fluid domain is solved in a small time-step locally on the background of a frozen large-scale temporal variation (Fig.5). A large-scale flow variable at time t_M is defined by taking a local time-averaging around t_M for a sufficiently large number of small time-steps N:

$$\tilde{U}_M = \frac{1}{N}\sum_{n=1}^{N} U(t_n) \tag{13}$$

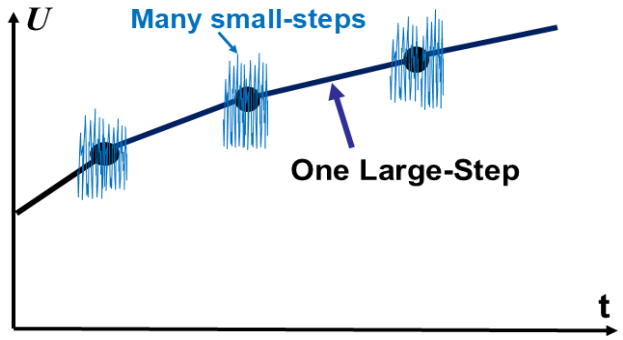

Figure 5: Dual Time-marching for Long-scale Transients

The flow governing equations can be expressed in a compact form:

$$\frac{\partial U}{\partial t} + R(U) = 0 \tag{14}$$

It is shown (He and Fadl [31]) that the dual time-scale fluid equations conditioned by the frozen large-scale time-gradient $(\frac{\partial \tilde{U}}{\partial t})_M$ becomes:

$$(\frac{\partial U}{\partial t})_n + R(U)_n = -(\frac{\partial \tilde{U}}{\partial t})_M \qquad \text{(n = 1, 2, ….., N)} \tag{15}$$

In the context of URANS, the local time-marching at a given large-scale time instant t_M is not time-accurate. It then reduces to a time-marching in pseudo time τ for sub-iterations at the given physical time instant as in the dual-timing formulation for a URANS- based transient CHT method (Fadl et al 2018 [32]. If N_{sub} is the number of sub-iterations, Eq.15 then becomes,

$$(\frac{\partial U}{\partial \tau})_k + R(U)_k = -(\frac{\partial U}{\partial t})_M \qquad (k = 1, 2, \ldots, N_{sub}) \qquad (15a)$$

It should be remarked that the augmented equations conditioned with the extra source term as expressed in Eq.15 is easy to solve at computational cost comparable to that of a conventional loosely coupled queasy-steady approach, as illustrated by He and Fadl [31] and Fadl and He [33].

The key advantage of the present method is that the quasi-steady assumption is no longer needed. More specifically, for the present dual time-marching CHT method, the source term in the fluid equation (RHS of Eq.15) ensures that the whole fluid domain is subject to the influence of the large-scale temporal gradient. In contrast, for a conventional quasi-steady CHT method, the large-scale temporal gradient is completely lost inside the fluid domain.

Here is an example of a transient natural convection process (Fig.6) subject to a fluid boundary ramp-up at different rates (Fadl and He [33]). To assess the impact of the conventional quasi-steady model, the present unsteady CHT method is also run in a quasi-steady mode by simply switching off the source term (RHS of Eq.15). The present unsteady solution is compared with the quasi-steady one for two cases at different temperature ramping-up rates for the inner wall of the fluid domain. For a slow transient (Fig.6b), the maximum discrepancy in the time averaged temperature on the outer wall surface between the unsteady and the quasi-steady model is about 20%. For the fast transient (Fig.6c), the maximum discrepancy rises to 45%. The quasi-steady assumption is clearly not valid in this case. In general, the quasi-steady assumption may not be safe in many seemingly long operations, parts of which consist of relatively short and rapid transients. The dual time-integration method provides a very simple and effective way to minimize the erroneous influence of a commonly adopted quasi-steady CHT.

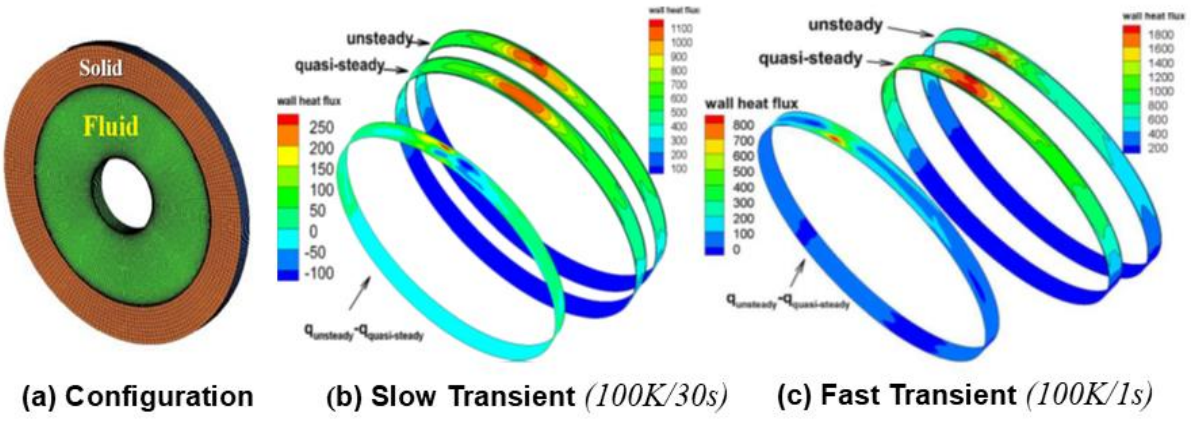

Figure 6: LES-CHT for Transient Natural Convection: Unsteady vs. Quasi-steady (*Time-average Heat Flux at Fluid-Solid Interface*, [33])

3.2. Time-Frequency Domain Fluid-Solid Coupling

3.2.1 Thermal Penetration from Fluid to Solid

For a semi-infinite solid domain subject to a temperature impulse on wall boundary, its penetration depth in solid δ_p depends on solid material property and time scale (Faghri et al [34]),

$$\delta_p = \sqrt{8\alpha_s t} \tag{16}$$

where α_s is the solid thermal diffusivity and t time scale. The unsteady temperature disturbance vanishes in the regions beyond the reach of the penetration. Hence, it does appear that temperature disturbances from fluid would get totally 'dumped' in the bulk of solid domain beyond the penetration depth. A question is, what happens to temperature unsteadiness on wall surface? If the wall temperature is unsteady, near-wall flow may be affected, regardless of how steady the bulk solid domain may be. We should also note the relation between the penetration depth and the wall temperature fluctuations. We may have a very small penetration depth with material of a very low thermal conductivity (e.g. a wall with Thermal Barrier Coating, TBC). Then energy conservation leads to much higher wall temperature fluctuations, as shown by He [35],[36], Fadl & He [33].

Fig.7 shows how solid temperature may respond to an incident thermal disturbance in terms of a given fluid temperature harmonic and a constant heat transfer coefficient. Three materials are considered: Steel (high conductivity), Titanium (lower conductivity) and Kapton (very low conductivity). The solid temperature harmonics are shown in Fig.7 (He, 2023 [5]). It is seen clearly that the low conductivity material may have a very small penetration, but the wall temperature unsteadiness can be very high, leading to a much higher possibility of affecting near-wall flow.

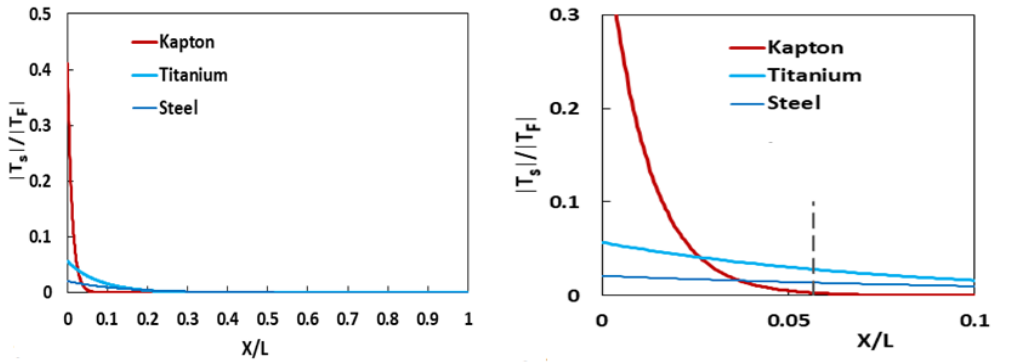

(a) Full Domain View *(Wall at x/L=0)*

(b) Close-up near Wall

(Dash line: penetration depth for Kapton)

Figure 7: Penetration of Fluid Temperature Harmonic (T_F) to Solid (L=0.5mm, f=1000Hz) [5].

A commonly adopted simple option is just to filter out all unsteadiness from the fluid domain. Couple a steady or time-averaged flow solution with a solid conduction solution (e.g. Sun et al [29], Errera and Baqué, [30], Duchaine et al [38], [39]). However, there is a wide range of self-excited unsteadiness encountered in many practical applications, e.g. from small-scale turbulent eddies in a turbine blade boundary layer to low frequency unstable thermal acoustic modes in combustors. We thus need be able to predict some unsteady CHT characteristics in a certain frequency range.

Therefore, there is a need for CHT methods to be able to predict unsteady CHT effects in general and the unsteady wall temperature fluctuations in particular, given the wide frequency spectrum of the unsteadiness encountered in various conditions of interest. As discussed earlier, a direct time-domain CHT solution will be prohibitively costly, so a time-domain CHT methodology in which both fluid and solid domains are time-accurately integrated must be avoided. But are there possible

alternatives by which the unsteady CHT effect in terms of wall temperature fluctuations can be predicted adequately at an affordable cost?

A framework for solving the steady and unsteady CHT parts interactively is thus envisaged as:

i) to have a baseline CHT method to couple a time-averaged fluid side with a steady solid conduction solution, similar to the conventional CHT methods.

ii) to have an 'add-on' unsteady CHT part capable of capturing wall temperature unsteadiness over a wide range of frequencies. However, this unsteady part should cost no more than the baseline steady-like CHT solution.

3.2.2. Fourier Model Interface and Baseline Time-averaged (0th Harmonic) Balance

The principal pathway taken here is to treat the CHT fluid-solid interface in frequency domain, rather than in time domain, as proposed by He and Oldfield [4] for modelling deterministic periodic unsteadiness in a temporal Fourier series. The question is, should we use a seemingly deterministic set of harmonics at their corresponding frequencies in a Fourier spectrum to represent seemingly non-deterministic/random turbulence unsteadiness?

In turbulence-resolving computations as well as in turbulent flow experiments, turbulence energy is commonly measured using a Fourier spectrum. A time-invariant harmonic in the context of a Fourier spectrum of seemingly 'random' turbulence may simply be interpreted as a statistically mean unsteady component at the frequency captured by Fourier transform over a long enough time period. In this regard it should not be surprising that a discrete Fourier spectrum is used for generating synthetic turbulence fluctuations as an inflow condition for LES, e.g. by Batten et al [40]. There have also been increasing applications of reduced order modelling (ROM) representations of turbulence, e.g. POD (Lumley [41]), DMD (Schmid [42]) and RESOLVENT (McKeon and Sharma [43]). These ROMs are shown to adequately represent the bulk kinematics and dynamics of random turbulence with a relatively small number of deterministic spatiotemporal modes. The successfully widespread applications of ROMs to turbulent flows provide extra support for using a Fourier spectrum in a fluid-solid interface treatment for a scale-resolving LES based CHT method.

We now use a discrete Fourier-spectrum with N_F harmonics to approximate a time-varying variable (e.g. temperature T with a complex-number $\widehat{\mathrm{T}}_n$ for its nth harmonic) for turbulent flow.

$$\mathrm{T}(x,t) = \overline{\mathrm{T}}(x) + Real\left(\sum_{n=1}^{N_F} \widehat{\mathrm{T}}_n e^{in\omega_0 t}\right) \tag{17}$$

where the time scale for the Fourier transform is given by a selected low frequency ω_0. For a fluid-solid interface (Fig.8), the fundamental physical condition is the continuity of heat fluxes, as well as temperatures from both sides to be the same on the wall.

$$q_f = q_s \tag{18}$$

In the Fourier spectral representation, the wall heat flux continuity is formally equivalent to the harmonic balance for each and every harmonic retained in the spectrum for the flux.

$$\left(\widehat{q_f}\right)_n = (\widehat{q_s})_n \qquad (n=0, 1, 2, \ldots\ldots, N_F) \tag{19}$$

The framework of the Fourier harmonic balance also provides a consistent basis for treating the steady/time-averaged part of the interface. Consider the harmonic balance for the zeroth harmonic:

$$\left(\widehat{q_f}\right)_0 = (\widehat{q_s})_0 \tag{20}$$

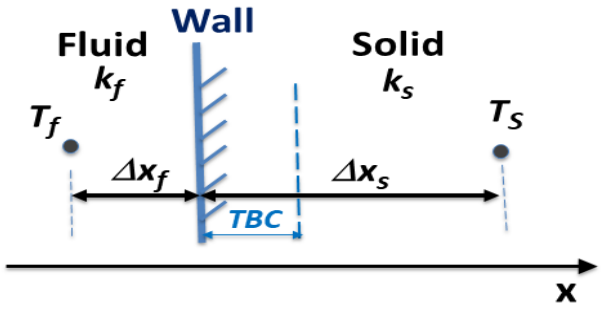

Figure 8: Variables at Mesh Points Adjacent to Fluid-Solid Interface

It is effectively the balance of the time-averaged fluxes from the fluid and solid sides, thus a manifestation of the physical flux continuity in terms of time-averaged variables. Effectively, the interface can be treated similarly to a steady CHT, once the time-averaged variables for the mesh points adjacent to the fluid-solid interface are available. A moving-average is used to update the time-averaging continuously on-the-fly as the solution proceeds (He 2019 [37]). With the physical temperature continuity at the interface, the time-averaged (the zeroth harmonic) wall temperature is obtained from the fluid and solid temperatures (T_f, T_s) at the mesh points adjacent to the interface (Fig.8):

$$\bar{T}_w = \frac{\left(\frac{k_f \overline{T_f}}{\Delta x_f} + \frac{k_S T_S}{\Delta x_S}\right)}{\left(\frac{\overline{k_f}}{\Delta x_f} + \frac{k_S}{\Delta x_S}\right)} \tag{21}$$

It should be noted that Eq. 21 only includes the nonlinearity in the time-averaging on the fluid side. For the solid side, the nonlinear effect due to the material property change with temperature is considered to be small, so the zeroth harmonic solid temperature T_s is uncoupled with the solid thermal conductivity k_s during time-averaging. Then, we have the baseline CHT solution established as the zeroth harmonic balance within the Fourier spectral framework.

Now we still need to figure out how the unsteady part for the solid domain can and should be dealt with. A field solution for each harmonic is equivalent to two steady field solutions for the in-phase and out-phase components respectively. If we have to retain a large number of harmonics, for instance, $N_F \sim O(10^2)$, a temperature harmonic solution in the solid domain can be a very substantial effort, thus is not appealing.

Bear in mind that it is the unsteady temperature at the wall surface which matters as far as the nonlinear fluid side is concerned. In addition, unsteadiness in a large frequency range will disappear in the bulk solid domain because of a limited reach of the corresponding penetration depth as discussed around Eq.16. As such, solving harmonics for a wide frequency range in the bulk solid domain will be largely a waste. What we would like to have is an efficient way to solve the unsteady wall temperatures, preferably without even needing the harmonic temperature field solutions within the solid domain. As introduced next, such an extremely efficient unsteady CHT interface treatment will be possible with a distinctive semi-analytical harmonic transfer function.

3.2.3. Harmonic Transfer Function for Fluid-Solid Interface

For many years, experimentalists have made extensive use of the transient solid temperature response to a flow impulse disturbance in their transient heat transfer measurements e.g. Schultz

and Jones [44], Doorly and Oldfield [45]. For a 1-D semi-infinite solid domain, there is a complex-number relation between wall heat flux harmonic and wall temperature harmonic for frequency ω:

$$\widehat{q_w} = \widehat{C_{Tq}}\widehat{T_w} \tag{22}$$

where the complex-number coefficient $\widehat{C_{Tq}}$ is effectively the temperature-heat flux harmonic transfer function for the wall surface. For a single layer solid domain, we have $\widehat{C_{Tq}} = \sqrt{i\omega}\sqrt{\rho c k}$, where $\rho, c \; and \; k$ are respectively the density, specific heat, and thermal conductivity of the solid. Note that Eq.22 was originally expressed in the Laplace space by Shultz and Jones [44], as used in the transient heat transfer experiments with non-periodic time responses. It was adopted in the frequency-domain with a detailed derivation for single and two-layer solids by He [37] and some validations by He and Oldfield [4]. Further discussions on the applicability of the 1D semi-infinite model for LES-CHT can be found in a recent chapter on CHT by He 2023 [5].

It should be pointed out that the harmonic transfer function is derived purely from the solid side, reflecting how the wall heat flux and temperature will have to vary in time (harmonically) accordingly for given solid material properties. In the context of unsteady CHT, the harmonic balance will have to 'constrain' the flux harmonic discretely computed from the fluid side, so that it will follow the same relation (Eq.22) because of the physical heat flux continuity, leading to: $\widehat{q_f} = \widehat{C_{Tq}}\widehat{T_w}$.

Next, we use the one-sided finite difference method to approximate the fluid heat flux harmonic $\widehat{q_f}$, leading to a semi-analytical interface condition for the wall temperature harmonic. For a Fourier spectrum of retaining N_F harmonics, the harmonic balance for each wall heat flux harmonic will lead to the following:

$$(\widehat{T_w})_n = (\widehat{TF_w})_n(\widehat{T_f})_n \qquad (\text{n} = 1, 2, \ldots\ldots, N_F) \tag{23}$$

$$(\widehat{TF_w})_n = \frac{\overline{k_f}}{\overline{k_f} + \Delta x_f \left(\widehat{C_{Tq}}\right)_n} \qquad (\text{n} = 1, 2, \ldots\ldots, N_F) \tag{24}$$

where $(\widehat{T_f})_n$ is the n^{th} fluid temperature harmonic at the fluid mesh point adjacent to the wall (Fig.8). $\overline{k_f}$ is the time-averaged thermal conductivity at the fluid mesh point. The complex-number $(\widehat{TF_w})_n$ is effectively a fluid-solid wall temperature transfer function for the n^{th} harmonic.

The distinctive semi-analytical wall temperature harmonic transfer function (Eq.24) demonstrates (unexpectedly perhaps) a remarkably useful capability. Now, as long as we have the fluid temperature harmonics at the fluid mesh points adjacent to the wall, we can get the corresponding wall temperature harmonics simply and directly with the wall transfer function $(\widehat{TF_w})_n$ (Eq.23). As a result, we no longer need any unsteady solid field conduction solutions. Consequently, the solid domain can now be solved completely as a steady conduction problem and time-marched with a much larger time-step (by 3-4 orders of magnitude). The steady solid temperatures and the time-averaged fluid temperature will enable the time-averaged wall temperature to be updated (Eq.21) as the zeroth harmonic baseline CHT interface condition.

For those fluid mesh points adjacent to a solid wall, the fluid temperature harmonics are continuously updated at each time-step with a moving-average discrete Fourier transform (He [37]). In the meantime, the instantaneous wall temperatures are constructed in time with the updated time-

averaged wall temperature and updated temporal harmonics. The continuously updated instantaneous wall temperatures will then condition the LES flow solution in time domain.

The extra computational cost for the unsteady part is now only a fraction of that for the baseline steady (time-averaged) CHT solution. This is chiefly because the DFT is only needed on the fluid side of the interface, essentially for one or just few 2-D surfaces in a 3-D fluid domain. The DFT updating is also only needed at each time step (rather than at each sub-iteration). Thus, when we retain as many as $O(10^2)$ harmonics, the extra cost will typically only be ~20-30% of that for the baseline steady (time-averaged) CHT. All considered, we now have a highly efficient unsteady CHT method in which the unsteady part acts like a small add-on part to the baseline steady CHT solution at only a fractional extra computational cost, as intended.

4. Two-scale Method: Macro & Micro Scales in both Fluid and Solid Domains

For a fluid domain bounded by a micro-structured wall, the two spatial scales of relevance are the small ('micro') scales with a typical characteristic length of a micro-structure element and the large ('macro') scales of a main flow path. A computational domain containing large number micro-structures can be discretised in a coarse base mesh. It is then further divided into a large number of local fine-mesh blocks around the micro-structures. As introduced in the previous lecture on the two-scale method, we would like to solve only one or a small number of local fine-mesh blocks and the global coarse mesh domain. We need to be reminded of the basic conflict. A local fine-mesh solution should provide a high resolution, but it however can only be useful if the local solution is properly conditioned by its surrounding. The global coarse-mesh domain may be well conditioned, but its solution can only be useful if it is adequately resolved. As such we need to find a way to make the global and the local domains interact with each other, as the primary motivation of the two-scale approach.

Some early efforts on two-scale RANS/URANS solutions of micro-structured wall-bounded flows (He, 2013 [35],[36]) clearly indicate the potential of iterative spectral mapping of a small set of fine mesh solutions in micro-element based blocks ('Block-spectral' mapping). Fig.9 shows the RANS results for an annular sector under a distorted inflow with 1600 'dimples' on the inner wall.

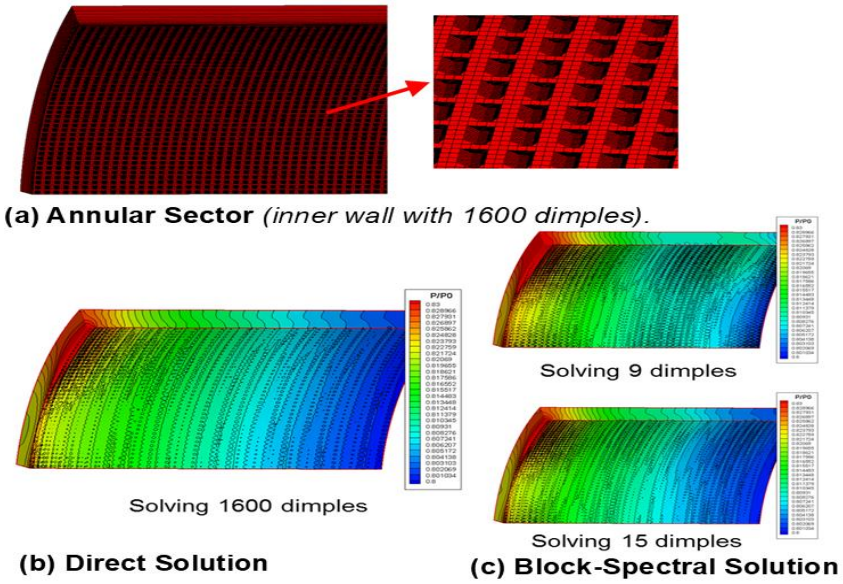

Figure 9: Dimpled Surface Configuration and Surface Pressures [35]

In the direct solution (Fig.9b), all 1600 dimples are solved with fine mesh. The two-scale block-spectral solutions (Fig.9c) indicate the potential of a far more efficient alternative of a comparable accuracy achieved by solving only 15 dimple fine-mesh blocks.

Another relevant application setting is effusion cooling. Fig.10a shows a simple annulus sector configuration (He [36]). The inner core domain with a high inflow temperature T_{01} is bounded by the solid layer. The cooler outer do6main has an inflow temperature $0.5T_{01}$. There are 992 simple shaped cooling holes linking the two domains. Fig.10b shows the baseline steady surface fluid temperatures on the outer boundary of the hot inner domain. Fig.11 shows URANS results for an unsteady inflow condition. The direct solution with all 992 holes solved in fine mesh (Fig.11a) agree very well with the two-scale 'Block-spectral' solution with only 8 holes solved in fine mesh (Fig.11b).

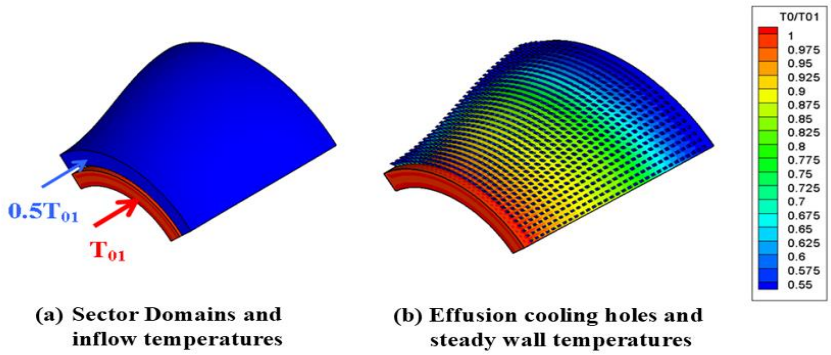

Figure 10: Effusion cooled sector configuration [36]

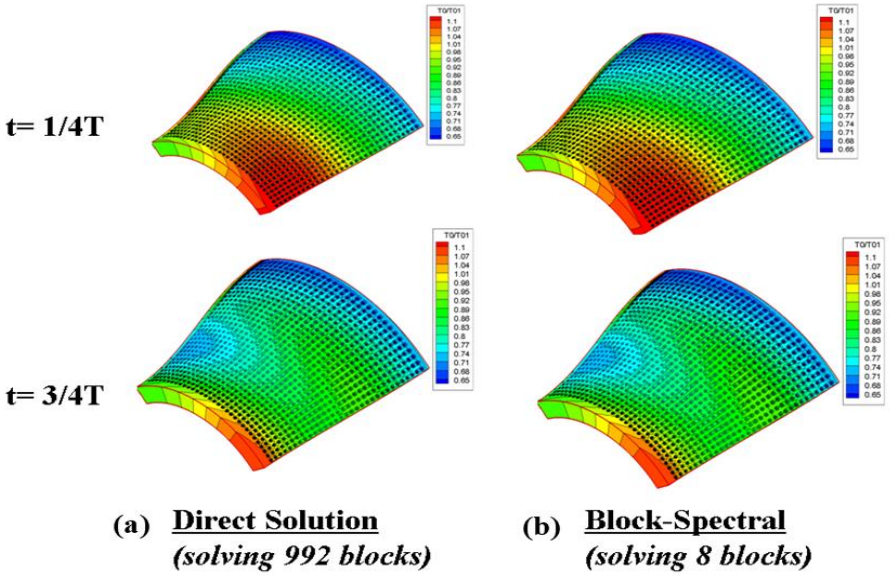

Figure 11: Unsteady wall temperatures (at two time instants in one period T) [36]

For LES, the two-scale method follows the same procedure as presented in the previous lecture on the two-scale LES for smooth wall. The only difference is that in this case, the fine-mesh block size is now dictated by the micro-structures. Hence, we solve only a small number of micro-element oriented fine-mesh blocks, to set a target solution for the coarse mesh. Source terms can thus be generated and propagated to the global coarse-mesh domain to drive the coarse-mesh solution. In the process of solving the coupled system, the global coarse-mesh and the local fine-mesh are made to correct each other, so that the converged solution for the coupled system will lead to a better conditioned local fine-mesh solution and an effectively better resolved global coarse-mesh solution.

An important further development is to extend the two-scale method to solid domain for solving the conduction equation. As discussed in the last section, thanks to the semi-analytical temperature harmonic transfer function at the fluid-solid interface, we now only need to solve a steady conduction problem in solid domain in the unsteady CHT. The solid conduction equation is essentially the same as the fluid energy equation, except for having zero velocities and solid property. Thus, the solid conduction equation is essentially discretized (in a finite-volume scheme) and solved (time-marched in a multi-step Runge-Kutta scheme) in the same way as the baseline fluid solver (He (37]).

Given the similarity between the solid and fluid solutions, it is now worth paying attention to the interpretation of the two-scale method working when applied to a solid conduction solution. For given material properties, the conduction equation is purely linear. When we have a fine-mesh solution U_f, satisfying $R_f(U_f) = 0$ on the fine-mesh, the volume-weighted spatial average of the fine-mesh equations on a coarse-mesh should also hold: $\widetilde{R_f(U_f)} = 0$. But we will still find that the space-averaged target solution on the coarse-mesh will not satisfy the coarse-mesh equation: $R_C(\widetilde{U_f}) \neq 0$. Similarly to the two-scale LES, we also adopt the direct mode and the inverse mode of the discrete solid conduction equation for the two domains respectively:

On global coarse-mesh ('Direct Mode'): $\frac{\partial U_C}{\partial \tau} + R_C(U_C) = S_s$ (25)

On local fine-mesh ('Inverse Mode'): $S_s = R_C(\widetilde{U_f})$ (26)

where the coarse-mesh equation is solved by time-marching in pseudo-time τ, driven by the space-averaging-led scalar source term S_s. The process here is seemingly the same as that for time-averaging the nonlinear flow equations. However fundamental to the generation of those extra 'Stress' terms is nonlinearity of the advection terms in the flow equations for random turbulence ('Reynolds stresses') or for periodic unsteadiness ('deterministic stresses' labelled for rotor-stator interactions by Adamczyk 1985 [47], or 'unsteady stresses' for vortex shedding by Ning and He 2001 [48]). However here for the solid domain in contrast, we have no nonlinearity as the conduction equation is purely linear for given material properties.

Given the above contrasting context, the source term generation when space-averaging the linear discrete conduction equation will have to have a different basis other than that for nonlinearity-led 'stress' terms when time-averaging the nonlinear flow equations. In the solid conduction setting, the scalar source term is generated simply and entirely due to numerical discretization errors. Consequentially the space-averaged solution from the fine-mesh will not satisfy the steady conduction equation discretised on the coarse-mesh. The source term (RHS of Eq.25) will thus be needed to balance out the numerical discretization errors, otherwise the fine-mesh solution projected on the coarse-mesh as the target would not be realizable in the coarse-mesh domain. The corrective scalar source term is simply generated 'in-situ' for the very coarse-mesh to be corrected. The inverse mode (Eq.26) taking the target solution mapped on the coarse-mesh as the input underscores that the imbalance of the coarse-mesh equation does originate entirely from discretization errors. It then follows that for the source terms generated to correct the global near wall discrete coarse-mesh flow equations in the two-scale LES, closing Reynolds stresses will be at best only part of the solution. As such, the effective correction source terms need to be 'mesh-informed', as they are.

5. Some Further Case Examples

5.1 Validation for Internal Ribbed Channel

The VKI internal flow experiment by Casarsa and Arts (2013) [49] and Cukurel et al (2013) [50] is judged to be a suitable case to validate the LES-CHT method for configurations with wall surface features [51], a simplified turbine blade internal cooling channel of a square cross-section with rib-roughened surface. The configuration of six ribs is taken (Fig.12a). Aerothermal characteristics are shown to be largely insensitive to the flow conditioning of ribs farther upstream than the adjacent one. Thus fine-mesh blocks are only embedded for the 3rd, 4th, and 5th ribs while the aerothermal parameters for the 4th rib are closely examined. The base coarse-meshes for these three ribs are shown for the fluid (Fig.12b) and solid (Fig.12c) domains respectively. The heat transfer effectiveness of internal ribbed wall is given by the effective enhancement (EF), Nu/Nu_0, ($Nu_0 = 0.023Re_{Dh}^{4/5}\,Pr^{0.4}$, the standard Dittus-Boelter correlation for turbulent channel flow).

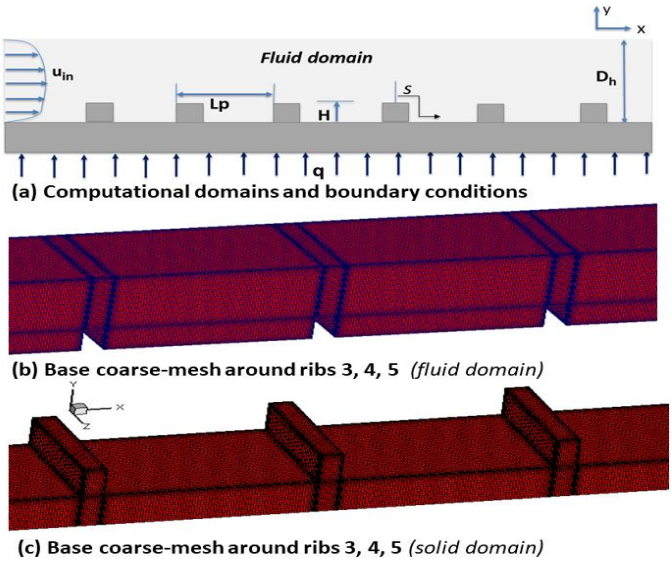

Figure 12: VKI ribbed channel configuration and base mesh [51].

5.1.1. Mesh Sensitivity

Different levels of refinement can be simply made by embedding different numbers of fine-mesh cells in each coarse mesh cell. Here we denote the cases with 8, 12 and 18 fine-mesh cells embedded in each base coarse-mesh cell as 'Embed8', 'Embed12' and 'Embed18' (Fig.13) respectively.

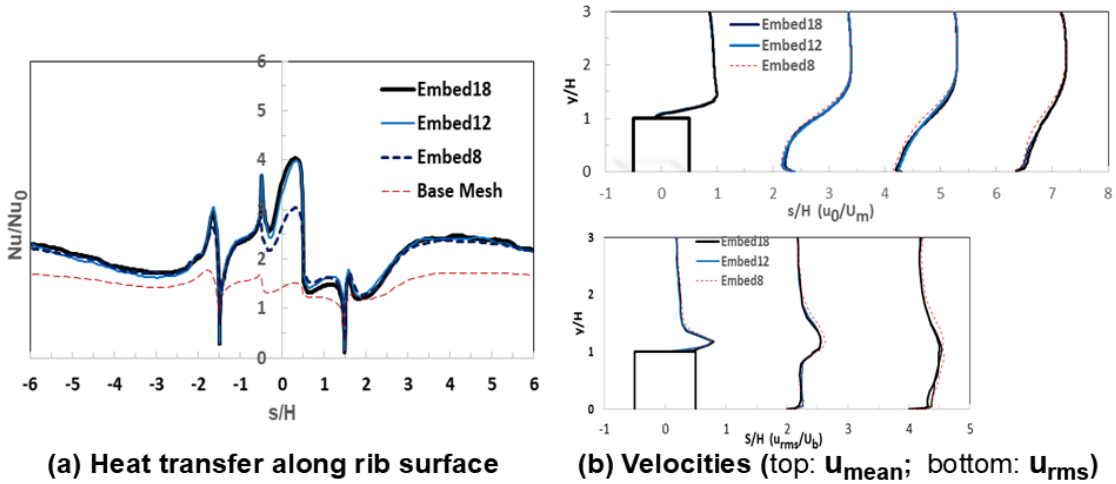

Figure 13: Mesh Sensitivity [51]

Generally, wall surface heat transfer (Fig.13a) is seen to be more sensitive to mesh density than velocity profiles (mean and rms, Fig.13b). Base mesh is clearly not nearly sufficient. Embed8 shows a reasonable mesh convergence for large part of the whole surface around the rib, but it is still under resolved around the rib top surface (-0.5 < s/H < 0.5). Embed12 and Embed18 indicate the range of the refinement required for an adequately mesh independent solution in this case.

5.1.2. Comparison with Experimental Data

The comparisons with the experimental data (Fig.14) lead to a similar observation: a reasonable comparison for the heat transfer (Fig14a), but a good one for both the mean and fluctuating velocities (Fig.14b).

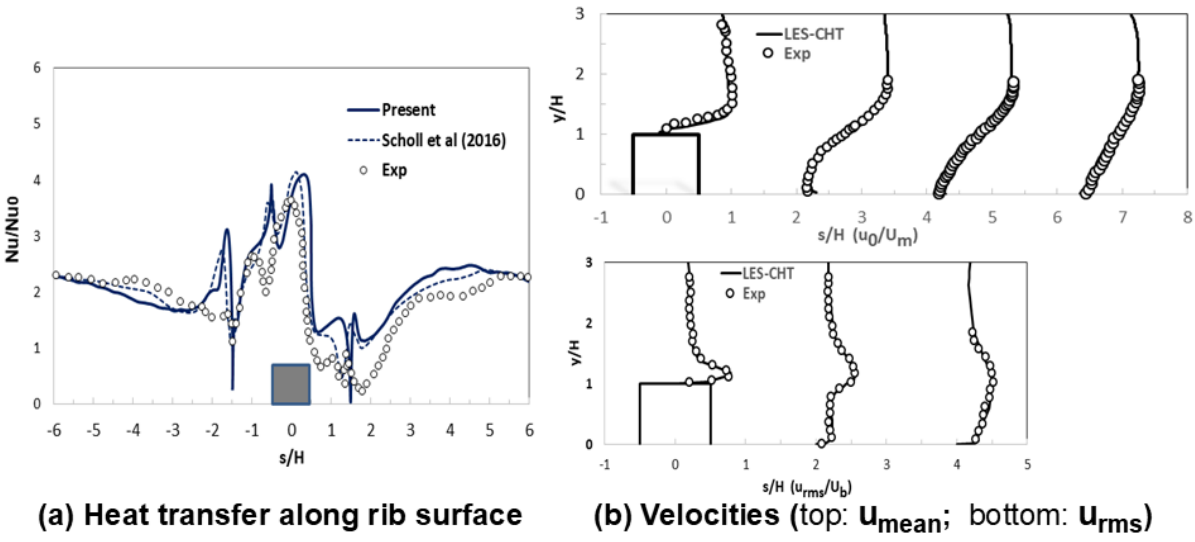

Figure 14: Comparisons with VKI experimental data [50] and CHT solution [52]

5.2. Two-scale Solutions for Micro-structured Wall

The test configuration considered is a steel slab with 100 micro-structures on its top surface subject to an inflow in the x direction (Fig.15). We will look at the computational tests in three settings:

a) Fluid-domain only,
b) Solid-domain only,
c) Fluid-solid coupled CHT.

The two-scale solutions with only local fine-mesh blocks will be compared with the direct full solution where the fine meshes are applied to all micro-structures. In addition, the source-term coupling effects will be elaborated by contrasting the two-scale solution with the solution with the same local fine-mesh but without the source-term coupling (denoted as '*one-scale*' solution).

5.2.1. LES for Turbulent Flow over Micro-structured Wall (Fluid-domain only)

For the flow domain, most boundary conditions are the same for this case and the fluid-solid coupled conjugate heat transfer case to be presented later. The key difference is that for this case, the adiabatic wall condition is applied to the bottom surface of the domain subject to micro-structures. All 100 micro-structures are of the same simple shape with a square base and a height/width of 0.5. The upper halves of the two side surfaces of each micro-element are tapered to the top surface by 10% of the width, as shown in the closeup of the micro-structure element (Fig.15a). The Reynolds number based on free stream velocity and micro-element height is 2800.

At the inlet, the boundary layer thickness is taken to be about 7 times of the micro-element height. In addition, a spanwise nonuniformity is introduced in a stagnation pressure distortion. We first get some idea of the mesh sensitivity for direct solutions before assessing the two-scale method. The base mesh is very coarse with only 3 mesh cells to cover the micro-element width and 2 cells for the height, so it clearly will be poorly resolved. Two fine-mesh embedding settings are thus examined: one with 5x5x5 fine mesh cells in each coarse cell ('Embed125') and the other finer one with 6x7x5 ('Embed210'). The time averaged velocity traverses are taken at the location downstream of the final row of micro-elements (90% domain length) and at the element height. Embed125 and Embed210 are in good agreement, and in a clear contrast to the poorly resolved base mesh result.

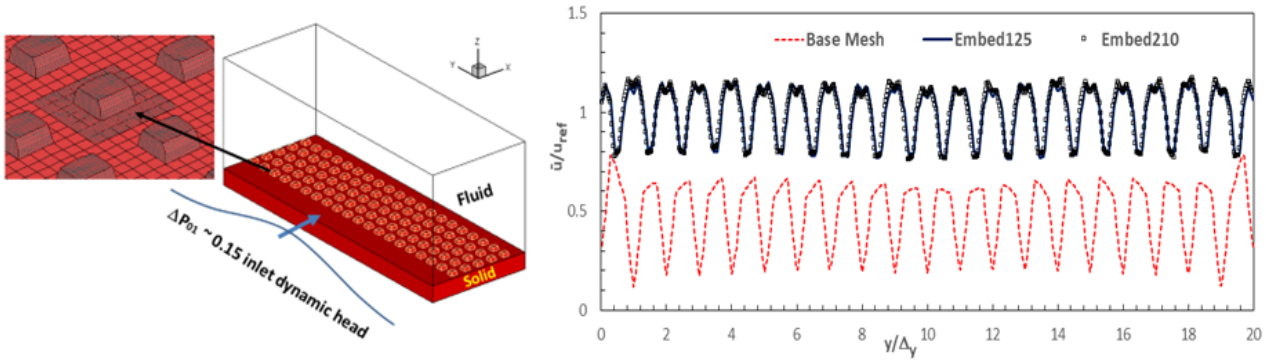

(a) Micro-structured Wall and Dual Meshes

(b) Mesh Sensitivity *(Downstream Traverse of Time-mean Velocity)*

Figure 15: Micro-structured Wall, Embedded Fine-mesh Block and Mesh Sensitivity [51]

Fig.16 indicates the turbulence scale-resolving capability of the all-fine-mesh direct solution (Fig.16a) compared to the two-scale solution (Fig.16b). In the two-scale solution the fine-mesh blocks are only embedded in a region covering three spanwise rows respectively.

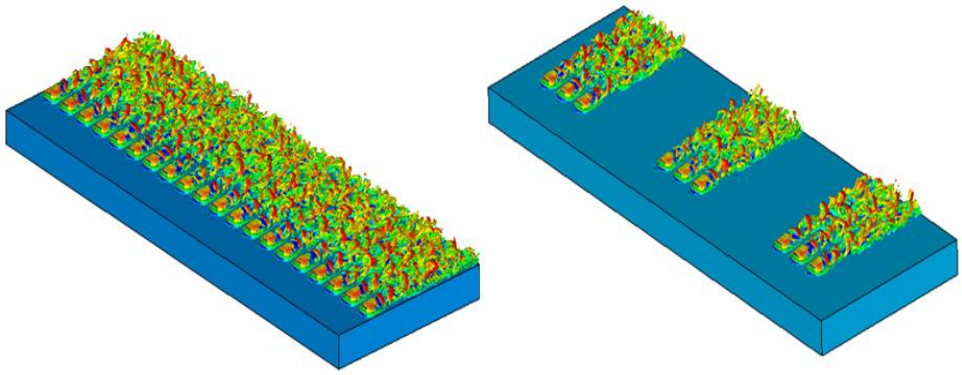

(a) Direct Solution (fine-mesh for 100 micro elements)

(b) Two-scale Solution (fine-mesh for 45 micro elements)

Figure 16: Scale-resolving turbulent structures, iso-Q surfaces coloured with velocity [51]

The time-averaged axial velocities are compared on the cut-plane at micro-element height (Figs.17a,b,c) and in a traverse at 90% domain length (Fig,17d) showing good agreement between the direct and two-scale solutions. The results show large discrepancies in the 'one-scale' solution with the same mesh as the two-scale one, underlining the importance of the source-term coupling.

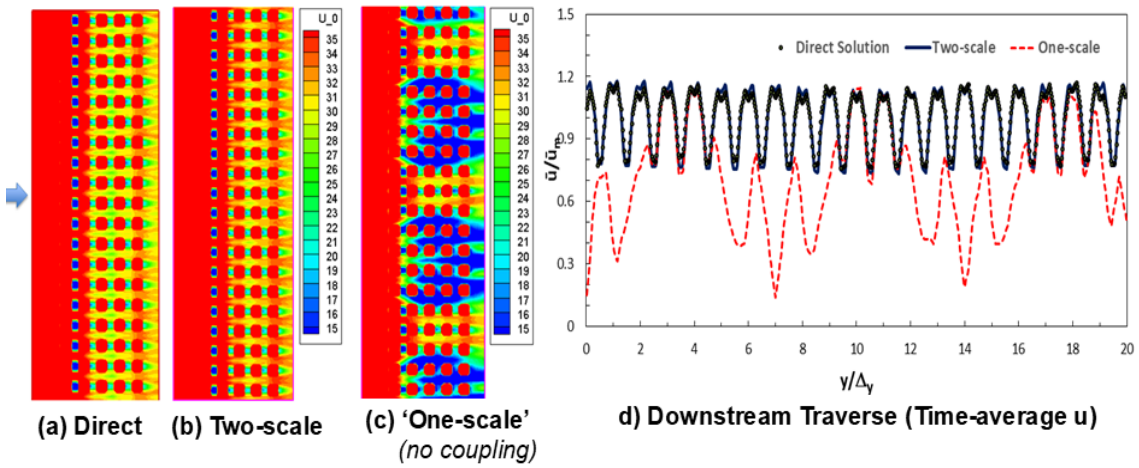

Figure 17: Time averaged velocities on micro-element top plane, and in downstream traverse [51]

5.2.2. Solid Conduction Solution for Micro-structured Layer (Solid-domain only)

An examination on the solid domain conduction solution is carried out before moving to the coupled CHT. The solid material is stainless steel. The solid domain configuration and boundary condition setup are indicated in Fig.18.

The 100 solid micro-structure elements are of the same shape as the in previous case (5.2.1) over the top boundary of the solid domain. The surfaces of the 100 micro-elements are subject to a specified wall temperature with a spanwise variation. The bottom boundary of the solid domain is subject to a specified low temperature $T_{Wbottom} = 0.6\,T_{01}$. Effectively the micro-elements act as 100 discrete heaters. The adiabatic condition is applied to all side surfaces of the domain and to the unheated flat parts of the top surface.

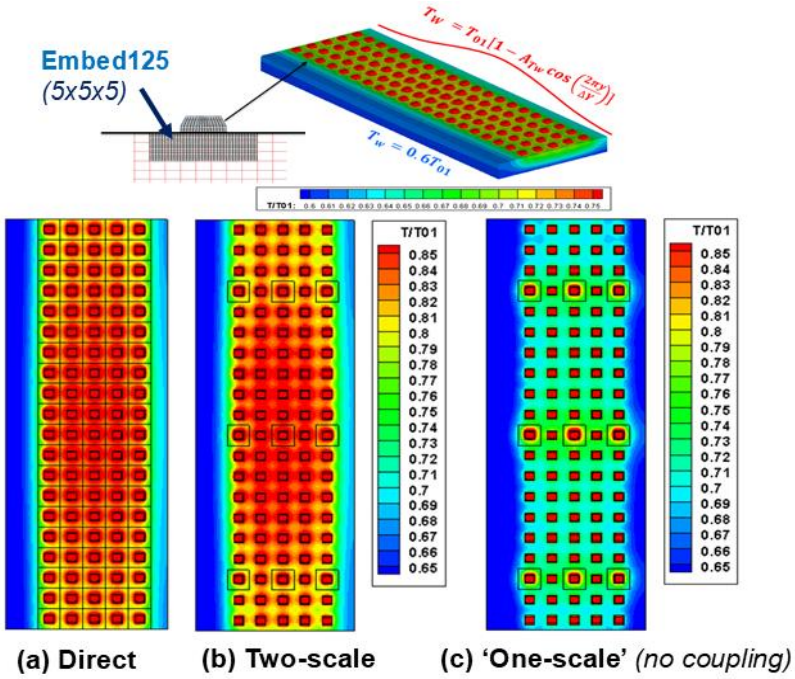

Figure 18: Solid Layer with Heated Elements and Temperatures on Top Surface Cut-plane [51]

In this case for the two-scale solution for solid conduction, only are 9 micro-elements locally embedded with the fine-mesh blocks. We can see that the two-scale solution (Fig.18b) is in good

agreement with the direct full fine-mesh solution (Fig.18a). The large discrepancies between the two-scale solution and the 'one-scale' solution (Fig.18c) underscore the inadequate resolution of the base mesh and the marked improvement that the two-scale source-term coupling can make. These results for a solid-domain-only case underline the importance of the numerical truncation errors, particularly illustrative in a setting having nothing to do with Reynolds-stresses, as discussed earlier in relation to the working of the source terms for the two-scale LES.

5.2.3. Conjugate Heat Transfer Solution (Fluid-Solid Coupled Domain)

Having examined the fluid-only and solid-only cases respectively, we now put the two domains together for conjugate heat transfer of this coupled micro-structured configuration. For the fluid thermal field, we compare the stagnation temperature contours on the cut plane at the middle height of the micro-elements, as shown in Fig.19a. The two-scale solution is again compared to the direct solution and the 'one-scale' solution (without the source-term coupling). The effectiveness of the source term coupling is again clearly underscored, without which the coarse-mesh regions are clearly very poorly resolved as shown by the 'one-scale' solution.

The solid surface temperature contours on the surface cutting through the bottom planes of the micro-structures are compared in Fig.19b. The result comparison again highlights the effectiveness of the underlying working of the two-scale method in addressing the basic conflict between a poorly resolved global domain and a poorly conditioned local domain.

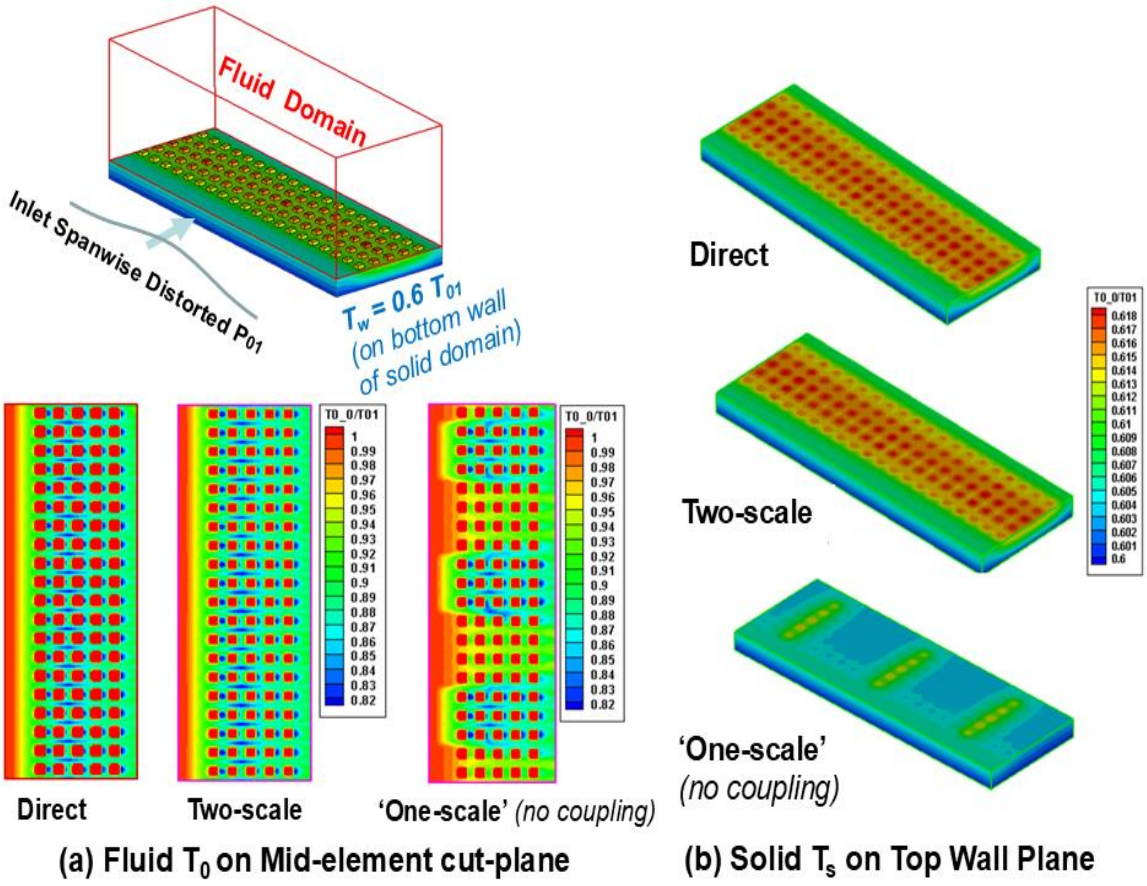

Figure 19: Fluid and Solid Temperatures from CHT solutions [51].

Closing Remarks

Fluid-solid coupled and wall-resolved method for micro-structured configurations is chiefly motivated by the prospect of 'Surface Design' selecting both shape and finish, potentially underpinned by the rapidly progressing Additive Manufacturing. The challenges lie in the scale disparity in space as well as in time. The avenue taken here is to address multi-scale problems by developing and applying multi-scale methods.

For time scale disparity between fluid and solid, firstly for long transients in practical start-up/shutdown and other flexible operation processes, a dual time-marching procedure is introduced to enable an efficient and accurate transient CHT solution. In contrast to conventional loosely coupled quasi-steady treatment of fluid side, the dual time-marching CHT approach includes the fluid domain unsteadiness in a source term during the CHT coupling with in minimal extra cost.

Secondly, for short scale turbulence fluctuations in scale-resolving LES based CHT, the solid domain is cast in frequency domain. The time-averaged (the zeroth harmonic) part is effectively obtained in the same way as a steady CHT. Wall temperature unsteadiness is simply and explicitly obtained from the fluid temperature harmonics through a distinctive semi-analytical temperature harmonic transfer function. Consequently, the solid domain can be solved as a steady conduction problem in its own time step, by $O(10^4)$ larger than the restrictive fluid time step.

For the spatial scale disparity issue, the two-scale method is employed in both fluid and solid domain. High local temperature gradients around large number micro-structure elements can be solved efficiently by resolving only a small number of fine-mesh blocks. The source term now drives the solution of the linear conduction equation (having nothing to do with Reynolds stresses) on a coarse-mesh towards its fine-mesh solution target. The results of the two-scale solid conduction solution underlines unambiguously the key role of the 'mesh-informed' source-terms in balancing out coarse-mesh under-resolution associated discretization errors.

Bear in mind that when a near-wall coarse-mesh is adopted (for cost-benefit) as in common wall modelled LES (or wall-function based LES), we have to face inherent numerical errors. Thus, for a near-wall coarse-mesh flow solution, Reynolds stress closure then becomes only part of the problem. Because of the inherent numerical discretization errors, it is argued that a correct Reynolds stress field (perfectly modelled or resolved) may not be sufficient to produce (correspond to) a correct flow field, and vice versa. Nor would a correct (mesh-independently generalizable) wall-function (physically modelled or machine-learned) be expected to consistently condition the coarse-mesh solution, leading to a correct flow field.

The developed CHT capability is validated for an internal cooling channel with a ribbed surface. For a test configuration with 100 micro-structures, a fluid domain-only, a solid domain-only and a coupled CHT solution are examined respectively. The test cases with two orders of magnitude local embedded mesh refinement underscore the potential of the two-scale LES-CHT approach.

References

1. Moffat, R. J., 1998 "What's New in Convective Heat Transfer?" International Journal of Heat and Fluid Flow, Vol.19, pp90-101.
2. He, L. 2023 "Spectral Heat Transfer Coefficient for Convection", International Journal of Heat and Mass Transfer, Vol.216, 124557.
3. Hickling. T. and He, L., 2023 "LES-CHT for a Rotating Cavity with Axial Throughflow." Journal of Turbomachinery, Vo1.145, Issue 6, 061006.
4. He, L., and Oldfield, MLG., 2011 "Unsteady Conjugate Heat Transfer Modelling." Journal of Turbomachinery, 2011, Vo1.133, No.3.
5. He, L., 2023 "Conjugate Heat Transfer: Some Fundamentals and Recent Progress". Chapter 2, *Advances in Heat Transfer*, Vo.55, Elsevier.
6. Jimenez, J., 2004 "Turbulent Flows over Rough Walls." Annual Revew of Fluid Mechanics. Vol.36, pp173-196.
7. Townsend, A. A., 1976 "The Structure of Turbulent Shear Flow". Cambridge University Press.
8. Flack, K.A. and Schultz, M.P., 2014 "Roughness Effects on Wall-Bounded Turbulent Flows". Physics of Fluids, Vol.26, 101305.
9. Thakkar, M., Busse, A., Sandham, N., 2018 "DNS of turbulent channel flow over a surrogate for Nikuradse-type roughness". Journal of Fluid Mech. Vol.837, R1.
10. Flack, K.A., 2018 "Moving beyond Moody". Journal of Fluid Mechanics, Vol.807, pp1-4.
11. Snyder, J. C., and Thole, K. A, 2020 "Effect of Additive Manufacturing Process Parameters on Turbine Cooling". Journal of Turbomachinery, Vo1.142, No.4.
12. Kapsis, M., and He, L., 2019 "Analysis of Aerothermal Characteristics of Surface Micro-Structures". Journal of Fluids Engineering, Vol.140, Issue 5.
13. Kapsis, M. et al., 2020 "Multiscale parallelized computational fluid dynamics modeling toward resolving manufacturable roughness". Journal of Engineering for Gas Turbines and Power, Vol.142(2), 021001.
14. Wilkins, P.H., Lynch, S.P., Thole, K.A. Vincent, T., Quach, S. and Mongilla, D, 2022 "Effect of a Ceramic Matrix Composite Surface on Film Cooling." Journal of Turbomachinery, Vo1.144, No.8.
15. Han, J. C., Dutta, S., and Ekkad, S. V., 2000 "Gas Turbine Heat Transfer and Cooling Technology". 1st ed., Taylor & Francis, Inc., New York.
16. Bogard, D. G., and Thole, K. A., 2006 "Gas Turbine Film Cooling." J. Propul. Power, 22(2), pp. 249–270.
17. Acharya, S., and Kanani. Y., 2017 "Advances in Film Cooling Heat Transfer". *Advances in Heat Transfer*. Vol. 49. Elsevier, pp91-156.
18. Krewinkel, R., 2013 "A review of gas turbine effusion cooling studies". International J of Heat and Mass Transfer, Vol.66, Part A, pp706-722.
19. Andreini, A., Facchini, B, Picchi, A., Tarchi, L., Turrini, F., 2014 "Experimental and Theoretical Investigation of Thermal Effectiveness in Multiperforated Plates for Combustor Liner Effusion Cooling"**.** Journal of Turbomachinery 136 (9), 091003.
20. Andreini, A., Cocchi, L., Facchini, B. Mazzei, L. Picchi, A., 2018 "Experimental and numerical investigation on the role of holes arrangement on the heat transfer in impingement/effusion cooling". International J of Heat and Mass Transfer, Vol.127, Part A, pp645-659.

21. Xu, R., Cheng Z., Jiang, P.X. 2023 "Fundamentals and recent progress of additive manufacturing-assisted porous materials on transpiration cooling". Journal of Global Power and Propulsion Society, Special Issue: Some Advances in Additive Manufacturing for Aerothermal Technologies pp19–48.

22. Takeishi, K, and Krewinkel, R., 2023 "Advanced Gas Turbine Cooling for the Carbon-Neutral Era". International Journal of Turbomachinery, Propulsion and Power, 8(3),19.

23. Campanaro, D. and He, L., 2023 "Impact of Wall Temperature on Aerothermal Characteristics of an Array of Surface Microstructures." Journal of Fluids Engineering, 145(2): 021203.

24. Diefenthal, M., Łuczynski, P. C. Rakut, M. Wirsum, W., T. Heuer, 2017 "Thermomechanical Analysis of Transient Temperatures in a Radial Turbine Wheel." ASME J. Turbomach., 139(9).

25. Łuczynski, P, D. Toebben, M. Wirsum, W. Mohr, F., and Helbig, K. 2019 "Unsteady Conjugate Heat Transfer Investigation of a Multistage Steam Turbine in Warm-Keeping Operation with Hot Air." ASME J. Eng. Gas Turbines Power, 141(1), p. 011005.

26. Maffulli, R.. Marinescu G., and He, L. 2020 "On the Validity of Scaling Transient Conjugate Heat Transfer Characteristics". Journal of Engineering for Gas Turbines and Power, Vol.142(3), 031021.

27. Oh, T. K. Tafti, D. K. and Nagendra, K., 2021 "Fully Coupled Large Eddy Simulation-Conjugate Heat Transfer Analysis of a Ribbed Cooling Passage Using the Immersed Boundary Method". Journal of Turbomachinery, Vol. 143, Issue 4, 041012.

28. Koren, C., R. Vicquelin, and O. Gicquel, 2018 "Multiphysics Simulation Combining Large-Eddy Simulation, Wall Heat Conduction and Radiative Energy Transfer to Predict Wall Temperature Induced by a Confined Premixed Swirling Flame". Flow, Turbulence and Combustion, Vol.101(1), pp77-108.

29. Sun, Z, Chew, J. W. Hills, N., Volkov, K. and Barnes, C., 2010 "Efficient Finite Element Analysis/Computational Fluid Dynamics Thermal Coupling for Engineering Applications". Journal of Turbomachinery, Vo1.132, No.3.

30. Errera, M. and Baqué, B., 2013 "A Quasi-dynamic Procedure for Coupled Thermal Simulations". International Journal for Numerical Methods in Fluids, Vol.72.

31. He, L. and Fadl, M., 2017 "Multi-scale Time Integration for Transient Conjugate Heat Transfer". International Journal for Numerical Methods in Fluids, Vol.83, Issue 12.

32. Fadl, M., He, L., Stein, P, and Marinescu, G., 2018 "Assessment of Unsteadiness Modelling for Transient Natural Convection", ASME Journal of Engineering for Gas Turbines and Power, Vol.140, Issue 1.

33. Fadl, M., He, L., 2017 "On Large Eddy Simulation based Conjugate Heat Transfer Procedure for Transient Natural Convection". Journal of Turbomachinery, Vol.139(11).

34. Faghri, A. Zhang, Y., and Howell, J.R., 2010 "Advanced Heat and Mass Transfer". Global Digital Press, Columbia, MO.

35. He, L., 2013 "Fourier spectral modelling for multi-scale aero-thermal analysis". International Journal of Computational Fluid Dynamics, Vol. 27, No. 2, p118–129.

36. He, L., 2013 "Block-Spectral Mapping for Multi-Scale Solution". Journal of Computational Physics, Vol.250, pp13-26.

37. He, L. 2019 "Closely coupled fluid-solid interface method with moving-average for LES based conjugate heat transfer solution". International J of Heat and Fluid Flow, Vol.79, 108440.

38. Duchaine, F., Corpron, A., Pons, L., Moureau, V., Nicoud, F., and Poinsot, T., 2009 "Development and Assessment of a Coupled Strategy for Conjugate Heat Transfer with Large Eddy Simulation: Application to a Cooled Turbine Blade". Int. J. Heat Fluid Flow, 30(6), pp. 1129–1141.

39. Duchaine, F., Boileau, M., Sommerer, Y., and Poinsot, T., 2014 "Large Eddy Simulation of Flow and Heat Transfer Around Two Square Cylinders in a Tandem Arrangement." J. Heat Transfer, 136(10), p.101702.

40. Batten, P., Goldberg, U. and Chakravarthy, S. 2004 "Interfacing statistical turbulence closures with large-eddy simulation". AIAA Journal Vol.42, No.3, pp485–492.

41. Lumley, J. L., 1970 "Stochastic Tools in Turbulence". Academic Press, New York.

42. Schmid, P. J., 2010 "Dynamic Mode Decomposition of Numerical and Experimental Data". J. Fluid Mech. Vol.656 (1), pp5–28.

43. McKeon, B. J. & Sharma, A.S., 2010 "A critical-layer framework for turbulent pipe flow". J. Fluid Mech. Vol.658, pp.336–382.

44. Schultz, D. L. and Jones, T. V., 1973 "Heat Transfer Measurement in Short Duration Facilities". AGARD AG-165, 1973.

45. Doorly, J. E. and Oldfield, M.L.G., 1987 "The Theory of Advanced Multi-Layer Thin Film Heat Transfer Gauges." Int. J. Heat Mass Transfer, Vol.30(6), pp. 1159–1168.

46. He., L, 2012, "Block-Spectral Approach to Film-Cooling Modeling". Journal of Turbomachinery, Vol.134. No.2.

47. Adamczyk. J. J., 1985 "Model equations for simulating flows in multistage turbomachinery". ASME Paper 85-GT-226.

48. Ning, W, and He, L., 2001 "Some Modelling Issues on Trailing Edge Vortex Shedding," AIAA Journal, Vol.39, No.5.

49. Casarsa, L., and Arts, T., 2002 "Aerodynamic Performance Investigation of a Rib Roughened Cooling Channel Flow with High Blockage Ratio". 11th International Symposium on Applications of Laser Techniques to Fluid Mechanics, July, 2002, Lisbon, Portugal.

50. Cukurel, B., Selcan, C., and Arts, T., 2013 "Film Cooling Extraction Effects on the Aero-Thermal Characteristics of Rib Roughened Cooling Channel Flow". ASME J. Turbomach., Vol.135(2), p. 021016.

51. He, L., 2023, "Two-scale Conjugate Heat Transfer Solution for Micro-structured Surface". International Journal for Numerical Methods in Fluids, Vol.95, Issue 8.

52. Scholl, S., Verstraete T., Duchaine, F., and Gicquel, L, 2016 "Conjugate Heat Transfer of Rib-roughened Internal Turbine Blade Cooling Channel using Large Eddy Simulation". International Journal of Heat and Fluid Flow, Vol.61, Part B, pp650-664.